Journal of Materials Processing Tech. 283 (2020) 116707

Contents lists available at ScienceDirect

Journal of Materials Processing Tech.

journal homepage: www.elsevier.com/locate/jmatprotec

Explosive welding of aluminium to stainless steel using carbon steel and niobium interlayers

G.H.S.F.L. Carvalho[a], I. Galvão[a,b], R. Mendes[c], R.M. Leal[a,d], A. Loureiro[a,*]

[a] CEMMPRE, Department of Mechanical Engineering, University of Coimbra, Portugal
[b] ISEL, Department of Mechanical Engineering, Polytechnic Institute of Lisbon, Portugal
[c] ADAI, LEDAP, Department of Mechanical Engineering, University of Coimbra, Portugal
[d] LIDA-ESAD.CR, Polytechnic Institute of Leiria, Portugal

ARTICLE INFO

Associate Editor: Prof R Mishra

Keywords:
Explosive welding
Solid-state process
Dissimilar welding
Interlayer
Impedance
Wave formation

ABSTRACT

This work aimed to study aluminium to stainless steel explosive welds produced using two different interlayers: carbon steel and niobium. The use of each interlayer was analysed and compared microstructurally and mechanically using many characterisation techniques. The final joints using both interlayers presented favourable interfacial microstructure: waves on both interfaces. However, the joint using the carbon steel interlayer showed the best mechanical properties compared to the joints using the niobium interlayer. All interfaces found on both welds were wavy. However, depending on the metallic alloy combination, the shape of the wave is completely different. The results suggest that the shape of the waves is influenced by the shock impedance mismatch of the materials being welded. The impedance mismatch parameter (IMP) developed for explosive welding in this work proved to be a compelling method to order metallic combinations in a single axis to estimate the tendency to form typical or curled waves. Typical symmetrical waves tend to develop less quantity of IMCs than curled waves. However, the mechanical tests performed did not detect differences that could have been caused by this difference.

1. Introduction

Aluminium and stainless steel are two of the most commonly used metals in engineering and always arouse scientific and industrial interest. The low density of aluminium and its ability to be alloyed with many elements (allowing it to reach a wide range of mechanical properties) result in a material with an excellent strength/weight ratio, together with other notable features such as good ductility at low temperatures, corrosion resistance, good electrical and thermal conductivity. Stainless steel, on the other hand, is a high alloyed steel that possesses remarkable properties like good corrosion resistance, being able to maintain good properties at high temperatures and also presenting excellent toughness even at cryogenic temperatures.

For the past decade, there has been a rapid rise in the interest in joining dissimilar materials that could deliver a set of properties that a single material is not able to do. Therefore, there is a growing interest in the joining of aluminium to stainless steels (Al-SS) because of their good corrosion resistance and excellent properties at low temperatures. These joints are used for many applications. Banker and Reineke (1993) reported the use of these joints for cryogenic pipe couplings; Chadwick and Jackson (1983) referred their use for connections to liquefied gas storage vessels; Aceves et al. (2015) used these joints for cryogenic pressurized hydrogen storage in hydrogen vehicles; and according to Kakimoto (2000) they are also used for transition joints, where it is necessary to change from one material to another, but direct arc welding is impossible or not feasible.

However, from the welding point of view, aluminium and stainless steel are not compatible alloys. According to Matthews et al. (1982), disparities in the melting temperature of about 100 °C do not require unconventional welding techniques, but the difference between the melting temperatures of iron and aluminium is greater than 850 °C, which makes the welding of these materials very complicated.

For this reason, complex welding combinations are often joined through connectors, which is usually the simplest way. However, the ideal way to join materials would be through processes that would not add weight to the final component. The main problem is that the welding of these complex combinations by the conventional fusion welding processes is often not feasible. For this reason, many solid-state welding processes such as friction stir welding (FSW), magnetic pulse welding (MPW), ultrasonic welding and explosive welding (EXW) have

* Corresponding author.
E-mail address: altino.loureiro@dem.uc.pt (A. Loureiro).

https://doi.org/10.1016/j.jmatprotec.2020.116707
Received 29 October 2019; Received in revised form 30 March 2020; Accepted 4 April 2020
Available online 08 May 2020
0924-0136/

been investigated for dissimilar welding more frequently in recent years.

Explosive welding is gaining attention in the last few years because this process has proved to be capable of welding aluminium to stainless steel consistently, such as the work of Aceves et al. (2015) and Guo et al. (2016a), and more recently the microstructural and mechanical characterisation performed by Carvalho et al. (2019a). However, the welding of these materials is highly complex even with EXW, and there are still many challenges in EXW regarding intermetallic formation and improving the final properties of the welded joint.

Hokamoto et al. (1993) were some of the first to address the complexity of aluminium to stainless steel welding and used a stainless steel interlayer to improve the weldability of the pair. They discussed aspects regarding energy distribution and intermetallic formation, and very interesting results were achieved. Aceves et al. (2015) highlighted the critical need for a reliable Al-SS joint for a transition joint for a cryogenic pressure vessel. Like most of the works, they chose to use interlayers between the aluminium and stainless steel. The authors used interlayers in the process, but in this case, a two-layered interlayer.

Guo et al. (2013) manufactured an Al-SS cylindrical joint that is significant for pipe transitions. Nevertheless, owing to the problems in the direct welding of aluminium to stainless steel, there was the presence of several defects at the interface resulting in a poor bonding quality. Later, Guo et al. (2016a) also directly welded aluminium to stainless steel. Again, an intermetallic layer was formed at the interface leading to poor mechanical behaviour.

More recently, Carvalho et al. (2018a) welded aluminium to stainless steel directly under several different conditions. They accomplished a consistent weld, but considering it was a weldability analysis; no mechanical evaluation was performed. However, the results provide guidelines for the choice of the best parameters and configurations for this welding.

After that, Carvalho et al. (2019a) evaluated the use of a soft aluminium interlayer, comparing the interlayered weld with direct joining. They found that although direct welding is possible, the mechanical properties are significantly improved using an interlayer. However, the final mechanical properties were not the best possible, considering that the fracture in the tensile/shear test occurred at the interlayer. Another relevant finding was to achieve a direct aluminium to carbon steel weld with excellent mechanical properties and a wavy interface. They claimed that this type of morphology helps to decrease the harmful effect of the intermetallic formation that is almost inevitable for this combination.

Taking into account that Carvalho et al. (2019a) obtained an excellent EXW joint of aluminium to carbon steel and that authors like Mendes et al. (2013) and Shi et al. (2017) showed that carbon steel is easily weldable to stainless steel, the idea of using a carbon steel interlayer was formed. If carbon steel, used as an interlayer, exhibits the same interfaces obtained when directly welded to aluminium and to stainless steel, there is a high probability of achieving excellent properties using a low-cost solution. However, considering that aluminium to stainless steel welding can be used for some applications such as cryogenic or nuclear, in which carbon steel presents many limitations, niobium could also be a good solution for use as an interlayer. Since it has also an extremely high melting temperature (2477 °C), this could result in few IMCs at the interface. In addition, both carbon steel and niobium have an intermediate thermal conductivity between the aluminium and the stainless steel, which could be an important asset to overcome the problems existing in direct welding of these metals due to the severe differences in their thermal conductivities, reported by Carvalho et al. (2018a).

However, despite the great industrial attention and the recent investigations addressing aluminium to stainless steel welding, no straightforward procedure has been developed and no optimum mechanical properties have yet been achieved. Furthermore, studies like those performed by Aceves et al. (2015) and Kakimoto (2000) show that these types of structures are usually manufactured with many interlayer plates or with expensive ones like nickel and silver, which makes the component heavier and more expensive. So, to fill these gaps in knowledge concerning this subject and seeking welded joints with excellent properties and that are feasible from the industrial point of view; the aim of this work is to study aluminium to stainless steel explosive welds produced by using two different interlayers: carbon steel and niobium. The welding characterisation was performed by: optical microscopy, scanning electron microscopy (SEM), energy-dispersive X-ray spectroscopy (EDS), electron backscattering diffraction (EBSD), tensile-shear mechanical testing, and nanoindentation.

2. Materials and methods

Explosive welds of aluminium to stainless steel, using carbon steel and niobium as the interlayers, were performed. The flyer plate was the AA6082-T6 aluminium alloy (hardness of 114 $HV_{0.2}$) and the baseplate was the AISI 304 stainless steel (hardness of 180 $HV_{0.2}$). For the interlayers, the low-carbon steel EN10130 (DC05) (hardness of 87 $HV_{0.2}$) and the ASTM B393 Type 2 unalloyed niobium (hardness of 53 $HV_{0.2}$) were used, both 1 mm thick.

Two series of explosive welds in a parallel full overlap joint configuration were performed. Both weld series were achieved using the same welding parameters and same explosive mixture: ANFO (density of 800 kg/m^3). The welding parameters are reported in Table 1.

The series are identified according to the interlayer that was used, following the “flyer – interlayer – baseplate” identification. So, “Al-CS-SS” is the identification for the “aluminium flyer – carbon steel interlayer – stainless steel baseplate”, while “Al-Nb-SS” identifies the “aluminium flyer – niobium interlayer – stainless steel baseplate”.

The samples were removed longitudinally to the welding direction for microstructural analysis. The samples were analysed in a Leica DM4000 M LED optical microscope. The microstructure was also assessed by SEM, in a Zeiss Merlin VP Compact field emission scanning electron microscope, equipped with EDS to estimate the chemical composition of the interface. In addition to these techniques, EBSD analyses were performed, in an FEI Quanta 400FEG ESEM/EDAX Genesis X4M field emission scanning electron microscope. The results obtained by EBSD were analysed with the software OIM Analysis.

The mechanical analysis of the joints was conducted by tensile-shear testing and nanoindentation. The tensile-shear tests were performed in quasi-static loading conditions (1 mm/min), using a 100 kN Shimadzu AGS-X universal testing machine; the geometries of the specimens tested were similar to Hoseini Athar and Tolaminejad (2015)’s work. A Digital Image Correlation (DIC) by a GOM Aramis 5M system was used to acquire the local strain fields in the tensile-shear tests. The preparation of the surface of the specimens for the imaging was done according to Leitão et al. (2012). The nanoindentation tests were performed by Micro Materials NanoTest equipment (30 mN load). The detonation velocity of the welds (which is the same as the collision point velocity for parallel configuration) was measured according to the

Table 1
Welding parameters.

	Weld series	
	Al-CS-SS	Al-Nb-SS
Flyer plate	AA6082	AA6082
Interlayer	DC05	Nb
Baseplate	AISI 304	AISI 304
Flyer-interlayer stand-off distance (mm)	4.5	4.5
Interlayer-baseplate stand-off distance (mm)	1.5	1.5
Explosive mixture	ANFO	ANFO
Explosive density ($kg\,m^{-3}$)	800	800
Explosive thickness (mm)	30	30
Explosive ratio	3.0	3.0

experimental procedure presented by Mendes et al. (2014).

3. Results

3.1. Collision parameters

For welds using interlayer plates, after the collision between the flyer plate and the interlayer, these two plates remain together before colliding with the baseplate, and the impact velocity on the base plate is the velocity of the set consisting of the flyer attached to the interlayer plate. The estimation of the impact velocity of the flyer (Vp_{flyer}) was computed through Gurney's equation for a one-dimensional problem in parallel configuration, discussed by Kennedy (1970). Although this equation is widely accepted, it must be taken into account that it presents some limitations. The equation ignores the acceleration of the flyer plate along the stand-off distance; hence, as reported by Kennedy (1970) and Patterson (1993), it represents only the terminal velocity. That said, the achievement or not of the terminal velocity and therefore, the proximity of the real value to the value computed with the equation will depend on the stand-off distance applied. Carvalho et al. (2017) also discussed some of the limitations of this approximation. The calculation of the impact velocity of the weld ($Vp_{flyer+interl}$) on the base plate was conducted according to Eq. 1. This approximation considers the perfectly inelastic collision theory and the momentum conservation.

$$V_{p\,flyer+interl} = \frac{m_{flyer} \cdot V_{p\,flyer}}{m_{flyer} + m_{interl}} \quad (1)$$

$Vp_{flyer+interl}$ is the impact velocity of the flyer and interlayer set ($m\,s^{-1}$); m_{flyer} is the mass of the flyer plate (kg); Vp_{flyer} is the velocity of the flyer immediately before colliding with the interlayer ($m\,s^{-1}$) and m_{interl} is the mass of the interlayer (kg).

Table 2 shows the welding result, the collision point velocities measured and the impact velocities computed for both weld series. The values in parentheses would be the impact velocities of a direct welding using the same parameters but without the interlayer. The use of the carbon steel and niobium interlayers reduced the impact velocity that would have occurred with direct welding by approximately 50%. Compared to the previous work undertaken by Carvalho et al. (2019a), in which a reduction of 25% was reached using an aluminium interlayer, the reduction of velocity using CS or Nb was two times greater than the previous one. This is justified by the higher density of steel and niobium compared to aluminium, Eq. (1) shows that a more massive interlayer will induce a smaller final impact velocity. The reduction in the impact velocity leads to a decrease in the energy dissipated in the collision.

3.2. Analysis of the interface

The results observed in Fig. 1 show that both welds revealed wavy interfaces for both sides of the interlayer, i.e. on the interface between the aluminium alloy and the interlayer, and the interface between the interlayer and the stainless steel. It is noteworthy that the interfaces are quite different when comparing the flyer/interlayer interface and the interlayer/baseplate interface. The behaviour is similar for the weld using the carbon steel interlayer (Fig. 1a) as well as for the weld using the niobium interlayer (Fig. 1b): the flyer/interlayer interface presents curled asymmetrical waves, and the interlayer/baseplate interface presents typical waves.

Table 2
Values of collision point velocity, impact velocity and the welding result.

Weld series	V_c ($m\,s^{-1}$)	V_p ($m\,s^{-1}$)	Welding result
Al-CS-SS	1860	311 (606)	Successful
Al-Nb-SS	1790	285 (592)	Successful

Fig. 2 shows in detail the interfacial waves of the upper interfaces of the Al-CS-SS weld (Fig. 2a) and the Al-Nb-SS weld (Fig. 2b). Concerning the top interface, there are similarities in morphology comparing the impact of the aluminium flyer with both the carbon steel and niobium interlayers. After etching, the microstructure indicates (arrows) that the carbon steel and the niobium have undergone a deformation according to a vortex rotation while the aluminium presented elongated grains next to the interface.

Regarding the bottom interfaces where typical waves were formed, Fig. 3 shows there are also similarities between the Al-CS-SS weld (Fig. 3a) and the Al-Nb-SS weld (Fig. 3b). Substantial deformation is found next to the interface and the depth to which one material penetrates another is essentially the same.

Despite the very different physical properties between carbon steel and niobium, the similarities are present in terms of the general morphology. However, Figs. 2 and 3 show that the welding using niobium presents a greater tendency (or ease) to form vortices, both in the union with aluminium (Fig. 2b) and in the union with stainless steel (arrows in Fig. 3b).

In order to characterise and confirm the deformation within the curled waves better, the samples were analysed by EBSD with Inverse Pole Figure (IPF). Fig. 4 shows the optical microscopy of the welds combined with the area analysed by EBSD for the Al-CS-SS weld (Fig. 4a) and the Al-Nb-SS weld (Fig. 4b). The EBSD proves the deformation of the materials in the waves, with the presence of elongated grains suggesting an intense deformation to form the curled morphology of the wave. Also, some small grains were nucleated next to the elongated and deformed grains, indicating some recrystallisation. As Fig. 5 indicates, these curled waves surround regions that present extremely high nanohardness values, which range between 6.3 and 14.1 GPa, for the Al-CS-SS weld (Fig. 5a), and between 1.8 and 19.3 GPa, for the Al-Nb-SS weld (Fig. 5b). The Al-CS-SS weld presented more uniform nanohardness values and a higher average nanohardness while the Al-Nb-SS weld presented a greater variation in nanohardness values and a lower average.

Fig. 6 shows the analysis by SEM. One of the main differences found between the Al-CS-SS weld (Fig. 6a and 6b) and the Al-Nb-SS weld (Fig. 6c and d) is the interfacial material found within the curled waves. While the Al-CS-SS weld presents several cracks, indicating brittleness, the Al-Nb-SS weld did not show any cracks. The interface between the aluminium and carbon steel was investigated in a comparable weld by Carvalho et al. (2018b) that found Fe_4Al_{13} and Fe_2Al_5 intermetallic phases by interpreting the Kikuchi patterns in an EBSD analysis. The interface between the aluminium and niobium was analysed profoundly by SEM and EBSD (using the Kikuchi patterns). The area inside the curled wave detailed in Fig. 6d was further analysed in Fig. 7. Fig. 7a suggests the presence of two different phases: a matrix (black) with another phase present in a smaller amount and dispersed in this matrix (grey). These phases were analysed by EBSD and the indexed Kikuchi patterns are shown in Fig. 7b and c.

The analysis indicates an aluminium matrix (black) with $NbAl_3$ phase (grey) dispersed through it. $NbAl_3$ is an intermetallic phase, but the average nanohardness was lower than the values found for the weld using the carbon steel interlayer (Fig. 5). The absence of cracks in the Al-Nb-SS weld compared to the Al-CS-SS agrees well with this result. Nevertheless, despite the identification of the two phases, it is crucial to understand that there is a significant difficulty in fully characterising the explosive welded interface in dissimilar welds, as discussed by Paul et al. (2013). Thus, it is not possible to affirm that other phases (especially non-equilibrium phases) are not formed throughout other regions of the interface.

When welding, it is necessary to bring the surfaces at an interatomic level to bond the materials together. In EXW, this level of interaction is supplied through heat, pressure and plastic deformation. Crossland (1982) claims that the strong impact of the plates leads to the formation of a metallic jet between the surfaces, which leaves clean virgin

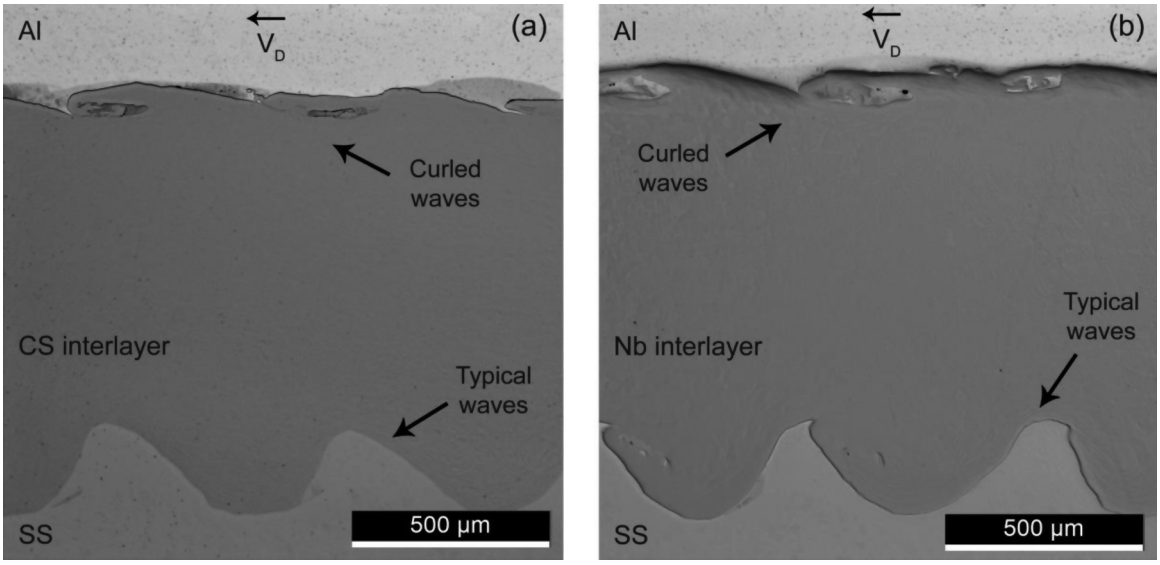

Fig. 1. Unetched optical microscopy of the weld with the CS interlayer (a) and the niobium interlayer (b). "V_D" represents the direction of the detonation propagation.

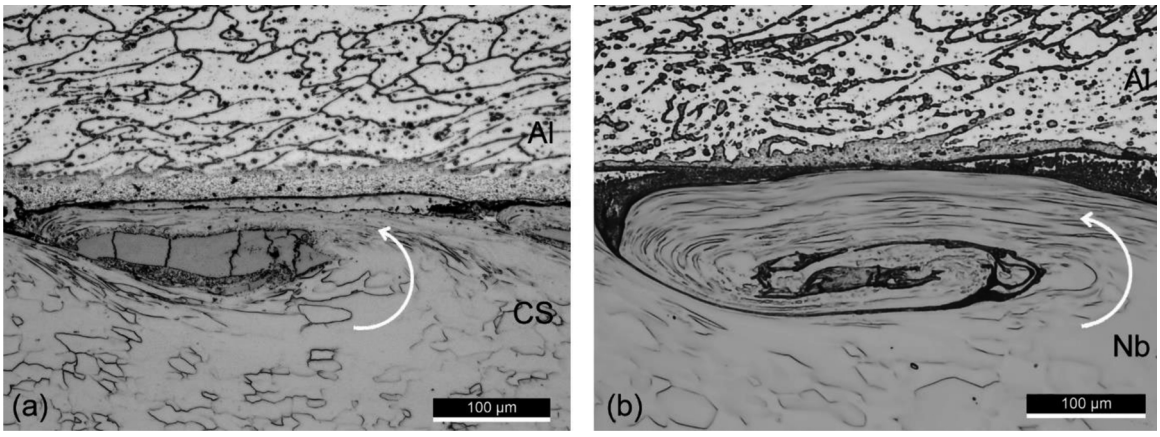

Fig. 2. Etched optical microscopy of the upper interface, with curled waves: CS interlayer (a) and niobium interlayer (b).

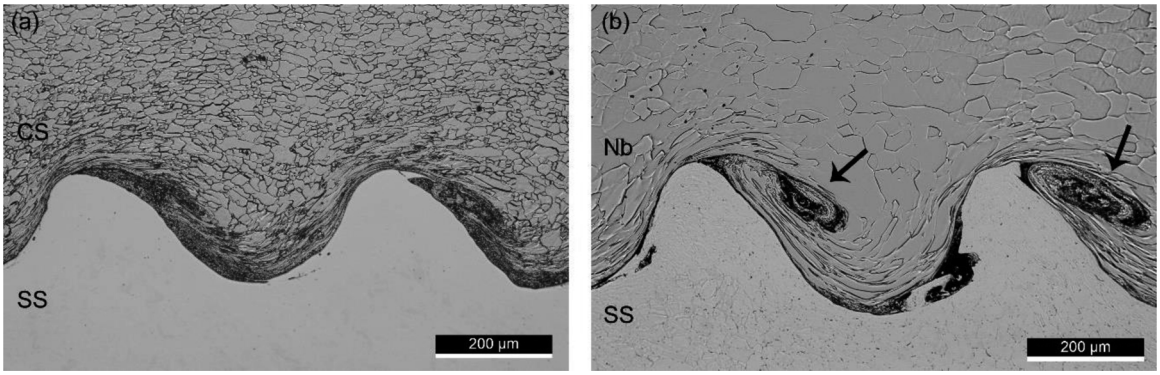

Fig. 3. Etched optical microscopy of the bottom interface, with typical waves: CS interlayer (a) and niobium interlayer (b).

surfaces. As pointed out by El-Sobky (1983), it allows the atoms of the materials to interact in the aftermath of the impact, resulting in an interatomic/metallurgical bond across the interface. Despite the same general bonding mechanisms, the bonding conditions were different between the typical wavy (Nb-SS andCS-SS) and the curled wavy (Al-Nb and Al-CS) interfaces. The different morphology of the interfaces is associated with differences in the interfacial phenomena, such as the interaction of the materials and the plastic deformation experienced, with influence on the mechanical interlocking of the materials. Moreover, another aspect that affects the interfacial bonding conditions is the existence of localised melting. This phenomenon was evident in the curled wavy interfaces, occurring preferentially inside the waves (Fig. 8a and b), but also in some regions surrounding the wave structure (Fig. 8a). Some evidences of localised melting are also discernible in the typical wavy interfaces (Fig. 8c and d).

The curled waves, which present an asymmetrical shape, are

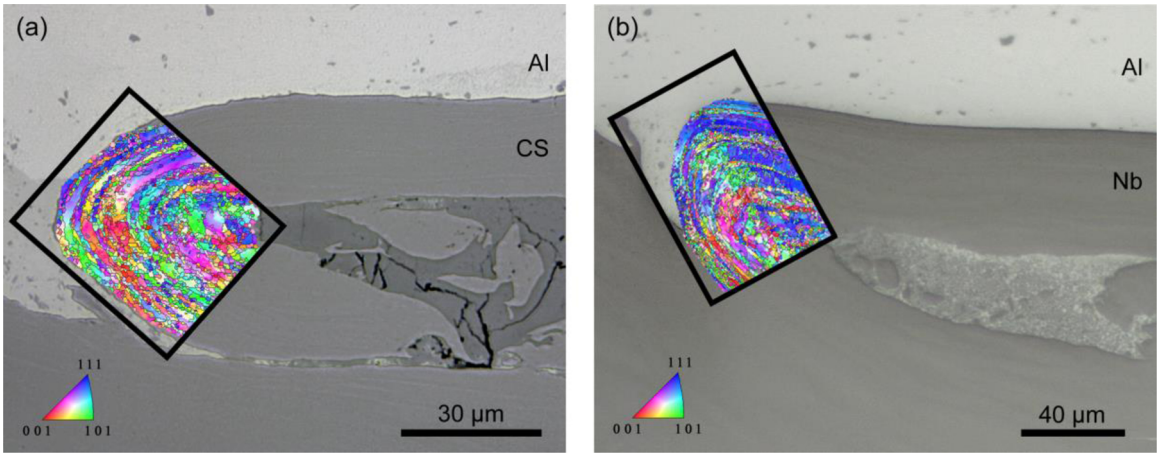

Fig. 4. Analysis of the curled waves by optical microscopy and EBSD with IPF: CS interlayer (a) and niobium interlayer (b).

composed mainly of one of the materials (one-sided penetration of the materials). On the other hand, the typical ones are more regular and symmetrical, and both materials participate in their formation (double-sided penetration of the materials). The mechanical interlocking is present in both interfaces, but due to their morphologies, they can result in different levels of interlocking. It is difficult to compare the two types of waves purely in terms of performance because their formation depends on the materials being welded. So, it is not possible to form the two interfacial morphologies for the same materials, parameters and configurations in order to compare them.

3.3. Mechanical behaviour

This section shows the mechanical behaviour of the welds. Table 3 shows the mechanical results and Fig. 9 illustrates the DIC images for the samples tested. Fig. 9 shows the distribution of deformation immediately before fracture (coloured image on the left) and the aspect after fracture (right image) for each sample. The samples with the carbon steel interlayer had the best performance and the highest maximum loads, with the deformation concentrated outside the weld region (Fig. 9a and b). The welds with the niobium interlayer presented slightly lower maximum loads, and the deformation concentrated at the interlayer (Fig. 9c and d). This concentration of strain at the interface matches well with the lower hardness of the niobium interlayer (about 87 $HV_{0.2}$) compared to the carbon steel interlayer (about 130 $HV_{0.2}$) after welding.

Fig. 10 shows the fractography of the samples, indicating that all the fractures were ductile. All the samples from the Al-CS-SS weld fractured outside the weld region with a ductile behaviour (Fig. 10a and b). The Al-Nb-SS weld fractured both in the aluminium, one near the weld region (Fig. 10c), and the other outside the weld region (Fig. 10d). All the samples that fractured far from the weld region (Fig. 10a and b for the Al-CS-SS weld, and Fig. 10d for the Al-Nb-SS weld) presented similar fracture mechanisms, with dimples from a tensile fracture. For the sample that fractured near the weld region, although the fracture also presented a ductile behaviour, the surface presented a different type of fracture with shear dimples (Fig. 10c).

The 1-Nb sample that fractured near the weld was further analysed by EDS in order to identify the specific region of the fracture. The EDS locations are identified in Fig. 10c and the chemical composition is shown in Table 4. The EDS analysis only showed the presence of aluminium for every location analysed. This fact indicates that, despite being near the weld, the fracture propagated only through the aluminium, outside the welding interface.

All samples presented excellent mechanical behaviour and even the weld that fractured near to the weld region had a maximum load relatively close to those fracturing in the weaker parent material (aluminium 6082). Moreover, none of the welds was found to fracture at the interface or through the interlayer, which proves the excellent welding results as a whole.

Comparing to the Al-SS welds from Carvalho et al. (2019a), produced by direct welding and with an aluminium interlayer, for which tensile-shear specimens with similar dimensions and geometry as in the current study were tested, the present samples had a quite improved mechanical behaviour. Unlike to the welds produced in the previous work, none of the welds was found to fracture at the interface or through the interlayer. Even the weld that fractured near to the weld region had a maximum load relatively close to those fracturing in the

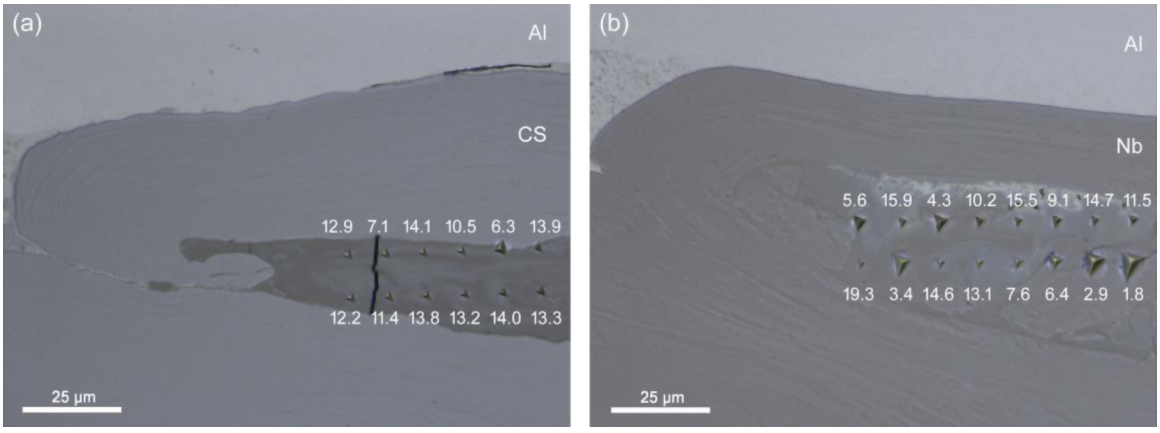

Fig. 5. Nanohardness measurements (GPa) of the mixed region inside the curled waves: CS interlayer (a) and niobium interlayer (b).

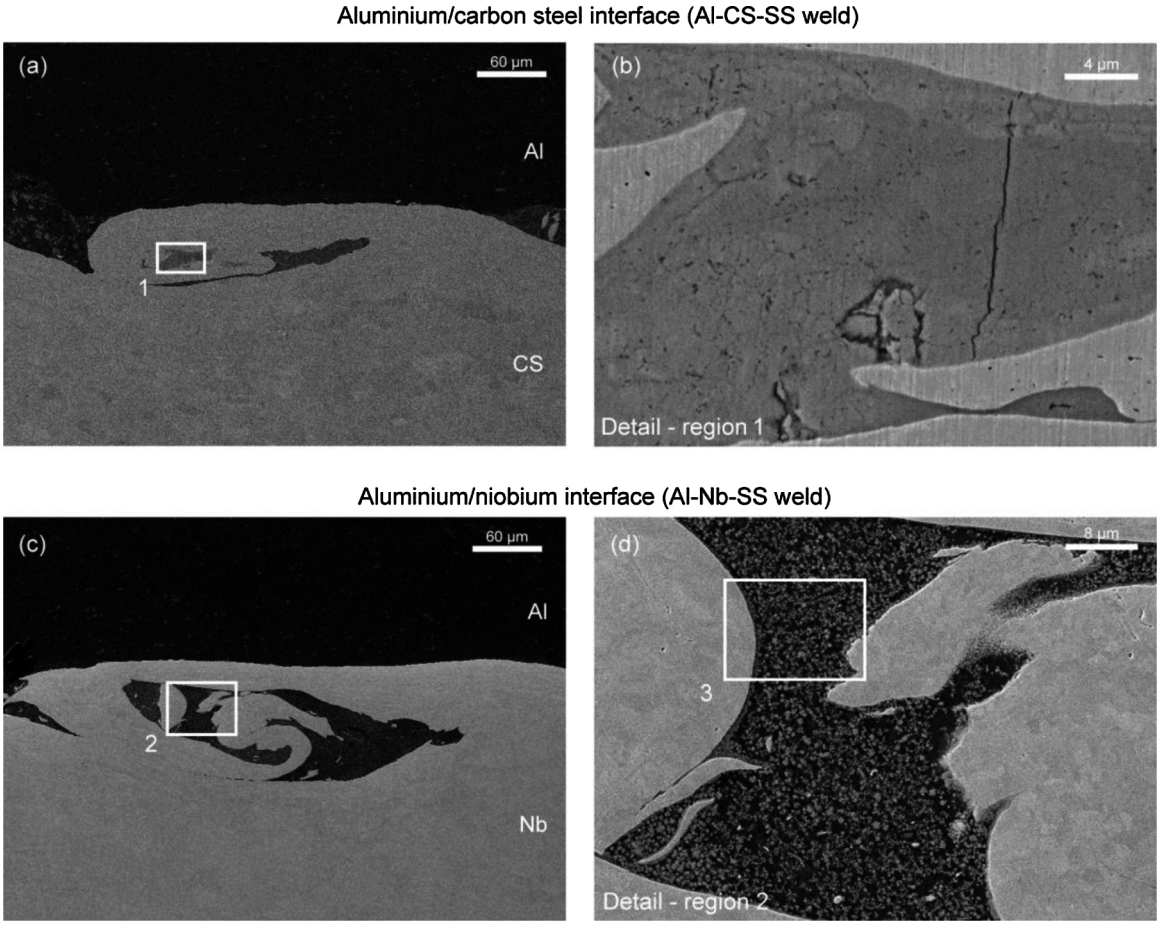

Fig. 6. SEM analysis of the curled waves: CS interlayer (a) and (b) and niobium interlayer (c) and (d).

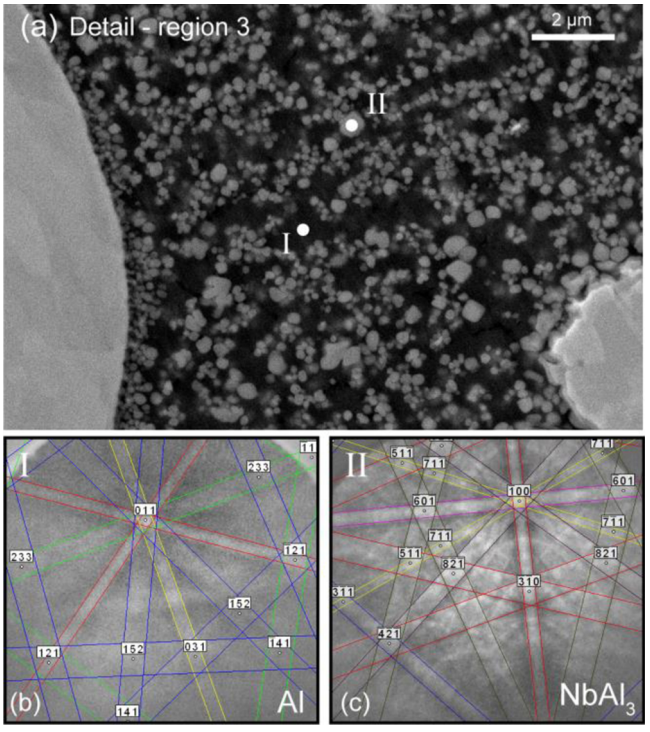

Fig. 7. SEM image with details from region 3 in Fig. 6d, indicating the locations of the EBSD analyses (a) and the respective Kikuchi patterns (b) and (c).

weaker parent material (aluminium 6082). None of the tests conducted in the present work presented brittle fracture.

4. Discussion

As reported by Carvalho et al. (2018a), in aluminium to stainless steel welding, the aspect that most hinders the welding is the difference in the thermal conductivity of the alloys. As observed in Table 5, both niobium and carbon steel have an intermediate thermal conductivity between aluminium and stainless steel. It means that the difference regarding this property is smoothed, improving the weldability. Furthermore, since some authors like Ouyang et al. (2006) claim that diffusion is much easier in liquid media and intermetallic formation is usually related to localised fusion, the melting temperature of the niobium alloys is much higher than that of the aluminium interlayer used in the previous work by Carvalho et al. (2019a) and that of the carbon steel, which resulted in fewer formation of IMCs at the interface of the Al-Nb-SS weld series.

Regarding the microstructural analysis, some considerations must be highlighted. As observed in Fig. 1, all interfaces were wavy. While the interface adjacent to the aluminium (Al/CS and Al/Nb) presented a curled morphology, the interface adjacent to the stainless steel (CS/SS or Nb/SS) presented typical symmetrical waves. The fact that both interfaces were wavy is already a microstructural improvement concerning the results obtained in Carvalho et al. (2019a) using an aluminium interlayer. In that work, the interface between the aluminium interlayer and the stainless steel was flat, and the presence of a wavy morphology would have improved the mechanical performance of the joint. In order to analyse the possibility of forming the interfacial waves, Carvalho et al. (2017) presented a dimensionless factor relating

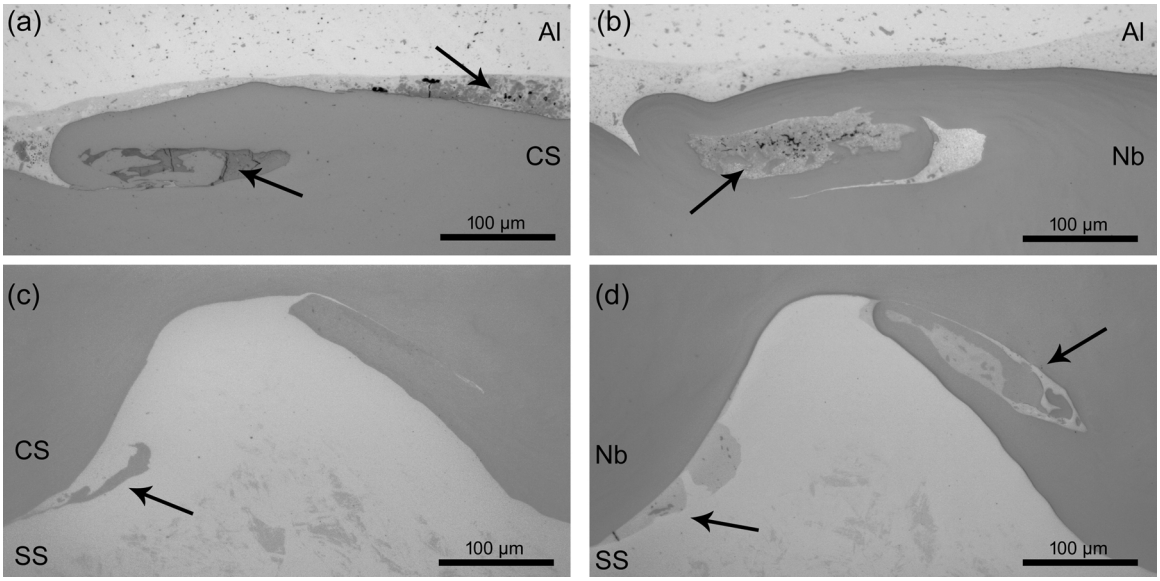

Fig. 8. Unetched optical microscopy of the weld with the CS interlayer (a) and (c); and the niobium interlayer (b) and (d). The arrows point to zones of possible melting.

the ratio of the physical properties of the flyer and the baseplate, which is called wave interface factor (WIF). This factor indicates whether a wavy morphology is likely or not to be achieved (values above approximately 5 only result in flat interfaces). Table 6 shows the calculation of the WIF and the expected results for all the weld series and interfaces.

Two relevant pieces of information can be observed in Table 6. The first is that, despite the significant differences between the aluminium flyer and both interlayers (CS and Nb), these differences are favourable for wave formation. Moreover, the properties of the interlayers are also favourable to form waves with the stainless steel baseplate. It indicates that both the carbon steel and the niobium alloy are favourable alloys to be used as interlayers in aluminium to stainless steel welds since they provide a desirable final interface morphology and microstructure.

Despite presenting the same general interfacial morphology (wavy), there are two significant differences between the upper and lower interfaces of both welds: the amount of IMCs formed and the shape of the waves. The upper interfaces in Fig. 2 (interface between flyer and interlayer) do not have the same amount of IMCs as the lower interfaces (interface between interlayer and baseplate) in Fig. 3. The differences in the physical properties of the pair being welded seem to affect how the alloys will mix and, consequently, the volume of regions with a mixed composition that will form. These regions, with the presence of multiple elements, may originate intermetallic phases.

The presence of IMCs is usually related to the presence of melting. However, the presence of an alloy with a lower melting point in itself does not justify the higher amount of IMCs formed at the upper interface. For instance, the works conducted by Paul et al. (2013), Hoseini Athar and Tolaminejad (2015) and later by Carvalho et al. (2018c, 2019b) addressing the welding of aluminium (low melting point material) to copper by explosive welding, present different amount of IMCs. Other welding combinations such as aluminium to titanium performed by Paul et al. (2018a) and aluminium to high alloy steel performed by Guo et al. (2016b) also present distinct IMCs quantities. In other words, it means that the presence of a low melting alloy does not indicate the absolute certainty of extensive intermetallic formation. The welding parameters, the interaction of the materials being welded (which is affected by their differences in physical properties), and the phenomena at the interface, will certainly affect the IMC formation and distribution at the interface. Therefore, the shape of the waves is also a factor of influence, and the features that lead to each type of wave should be investigated.

Despite indicating the possibility of the formation of a wavy interface, the WIF does not indicate the type of wave that will be formed. Observing Table 5, when materials with similar densities were welded (Nb-SS or CS-SS), typical waves were formed, as may be seen in Fig. 3. When there were significant differences in densities, asymmetrical curled waves, with a coiled morphology are formed as observed in Fig. 2. This proves the importance of the density of the materials in the formation of waves and, more importantly, the relevance of the difference in density between flyer and baseplate. This fact agrees well with the present results, but if this analysis is extrapolated to other dissimilar combinations that form waves at the interface, this approach may be generalised to dissimilar welds as a whole.

Therefore, an extensive data collection was made from the results of the present investigation and other results available in the literature. From the literature available, we sought works in which dissimilar EXW was performed and wavy interfaces were identified and where it was possible to define whether the wave was typical/symmetrical (as in Fig. 3) or curled (as in Fig. 2). Then, the physical properties of the base materials were studied in order to understand which factors lead to welds resulting in such diverse wave morphologies. Eighteen different

Table 3
Results of the tensile-shear tests.

Weld	Sample	Maximum load (kN)	Fracture region	Fracture	Figure
Al-CS-SS	1-CS	11.4	Outside the weld (Aluminium flyer)	Ductile	Fig. 9a Fig. 10a
	2-CS	11.5	Outside the weld (Aluminium flyer)	Ductile	Fig. 9b Fig. 10b
Al-Nb-SS	1-Nb	8.8	Near to the weld[a] (Aluminium flyer)	Ductile	Fig. 9c Fig. 10c
	2-Nb	11.0	Outside the weld (Aluminium flyer)	Ductile	Fig. 9d Fig. 10d

[a] Near the weld, but outside the welding interface.

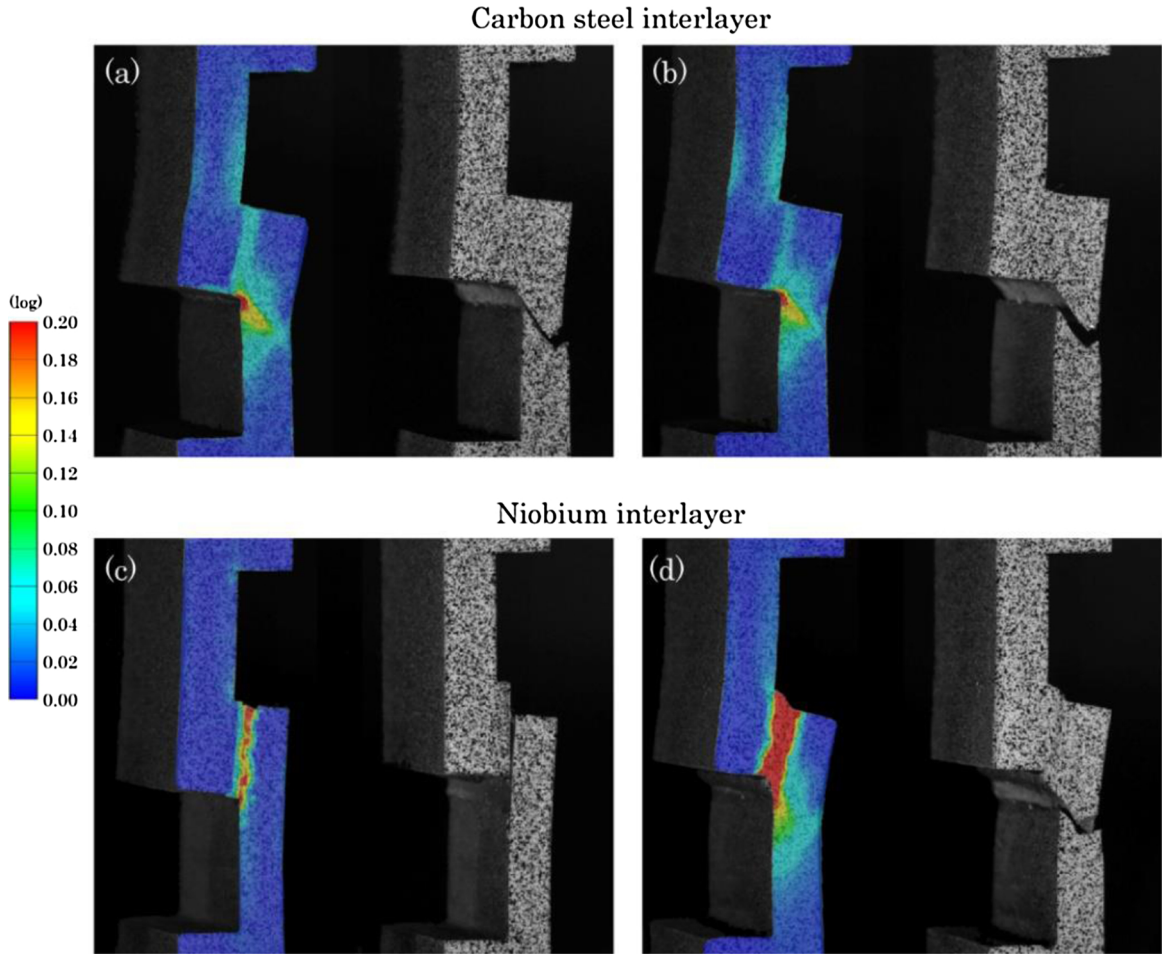

Fig. 9. DIC of the weld with the CS interlayer: samples 1-CS (a) and 2-CS (b); and with the niobium interlayer: samples 1-Nb (c) and 2-Nb (d).

dissimilar welding combinations were studied, seven with typical waves (Table 7) and eleven with curled ones (Table 8). These two tables show that the metallic combinations (and their respective physical properties) are very diverse. So, there is no simple pattern for the relationship of the properties between the flyer and base that could differentiate the welds with typical waves and the welds with curled ones easily.

However, despite not having a clear pattern regarding the relation between the properties of the plates, the present work showed that the materials with similar densities resulted in typical waves and more significant variation of densities resulted in curled waves. Therefore, the influence of density was deepened. One of the difficulties in analysing density in this situation is to realise its physical meaning within the phenomena that happen at the interface of an explosive weld. One way to relate density to explosion welding phenomena is to use the shock impedance concept.

According to Grady (2017)'s interpretation, the impedance of a material can be defined (in a simplified way) as the velocity at which the propagating wave subsumes the mass of the body. The shock impedance (Z) can be calculated with the product of the material's density and the bulk sound velocity propagation in it. Considering that besides the density, the impedance considers wave propagation, it is more intuitive to relate this property to the welding than the density alone. In Table 9, the impedances of each material were approximately calculated considering their densities and the bulk sound velocity propagation in the material.

In order to analyse and relate the impedances of the plates, the ratio of the impedances (Z_{ratio}) between the flyer and the baseplate (flyer's impedance / baseplate's impedance) was calculated for each metallic combination (Eq. (2)). This ratio illustrates the disparity of impedances between the flyer and the base: the further away from 1, the higher the disparity between the ratios (the ratio for equal impedances would be 1).

It is known that if the impedances of the welded plates are completely equal in an impact, no wave reflection will take place (Chen and Chandra, 2004). However, a higher impedance mismatch between the materials results in a larger magnitude of the reflected wave. This means that substantial differences in impedance can significantly change the behaviour of the shock waves at the interface during impact on welding.

Since a ratio of 1 indicates a combination of materials of equal impedances, to quantify the impedance mismatch between flyer and baseplate, the distance between the impedance ratio of each weld and the value of 1 was calculated (both for ratios greater than 1, i.e. flyers with higher impedance; and for ratios lower than 1, i.e. baseplates of higher impedance). This calculation follows Eq. (3) and it considers the absolute value of the difference from 1. This distance represents how "far" a given metallic combination is from an impact of a metallic combination of equal impedances. This calculation can be called the impedance mismatch parameter (IMP) for explosive welding.

$$Z_{ratio} = \frac{Z_{flyer}}{Z_{base}} = \frac{\rho_{flyer} \cdot C_{b\,flyer}}{\rho_{base} \cdot C_{bbase}} \quad (2)$$

Z is the impedance (kg m^{-2}s^{-1}), ρ is the density (kg m^{-3}) and C_b is the bulk sound velocity propagation in the material (m s^{-1}).

$$IMP = |1 - Z_{ratio}| \quad (3)$$

The calculation of the IMP makes it possible to order any welding

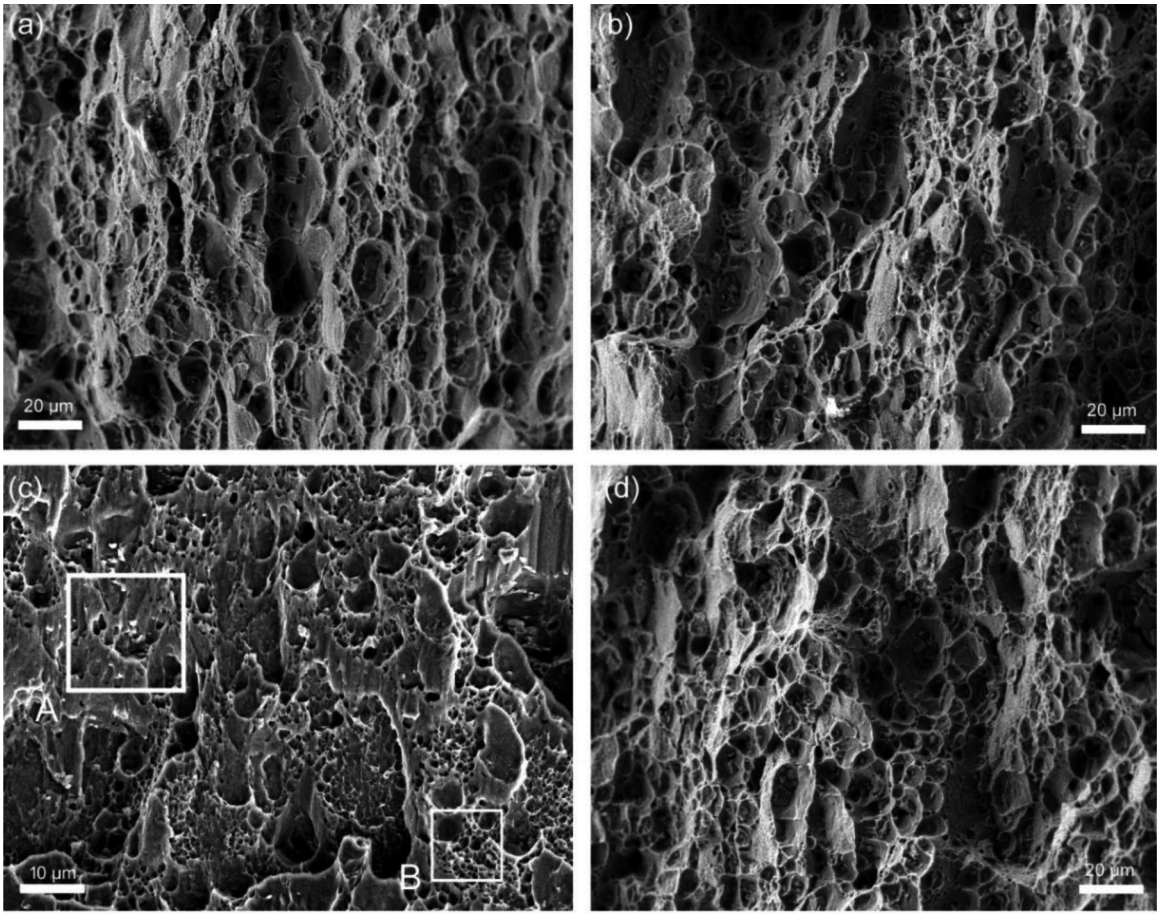

Fig. 10. SEM analysis of the fracture surfaces of the weld with the CS interlayer: samples 1-CS (a) and 2-CS (b); and with the niobium interlayer: samples 1-Nb (c) and 2-Nb (d).

Table 4
Chemical composition (atomic %) of the fracture surface of the sample 1-Nb.

ID	Weld series	Al	Mg	Si
A	Al-Nb-SS	98.3	0.8	0.9
B		98.6	0.6	0.8

combination on a single axis, which is a significant advantage. Table 9 presents these values in descending order from highest to lowest, including similar welds (SW) that would present an IMP of zero regardless of the material. As the distance to the value of 1 increases, i.e. the impedance mismatch increases, the waves tend to be curled. There is a threshold between typical wave welds and curled waves that may be related to the impedance disparity. The welds with typical waves are all grouped at the bottom of the table. Above certain impedance mismatch, the waves found for the metallic pair transit to curled ones. Fig. 11 presents the results in Table 9 graphically. The results are clearly separated into the welding group that forms curled waves and the group that forms typical waves.

It should be noted that the welding parameters also have a significant effect on the weld interface and can dictate either the non-appearance of waves or even "intensify" the shape of the wave. However, this approach only considered welds with wavy morphology, i.e. welds in which the parameters for wave formation have already been met.

In order to understand the IMP from a physical perspective better, the impedance might be related to some interfacial phenomena. The

Table 6
Calculation of the WIF, according to Carvalho et al. (2017).

	Al-CS-SS		Al-Nb-SS	
	Al-CS interface	CS-SS interface	Al-Nb interface	Nb-SS interface
WIF	0.15	1.05	0.08	1.89
Expected interface by the WIF	Wavy	Wavy	Wavy	Wavy
Interface obtained (Fig. 1)	Wavy	Wavy	Wavy	Wavy
Type of wave	Curled	Typical	Curled	Typical

Table 5
Physical properties of the welded alloys.

	Melting temperature (°C)	Thermal conductivity ($W\,m^{-1}\,K^{-1}$)	Density ($kg\,m^{-3}$)
AA6082 (ASM Handbook, 1990a)	650	180.0	2700
AISI 304 (ASM Handbook, 1990b)	1400	16.2	8000
DC05 (Spittel and Spittel, 2009)	1497	66.9	7860
Niobium (ASM Handbook, 1990a)	2468	52.3	8570

Table 7
Dissimilar welds with typical waves and their physical properties according to Gale and Totemeir (2004).

Combination (Flyer-baseplate)	Melting temperature (°C)		Thermal conductivity ($W\,m^{-1}\,K^{-1}$)		Density ($kg\,m^{-3}$)	
	Flyer	Base	Flyer	Base	Flyer	Base
Fe-SS (current work)	1538	1400	80.4	16.2	7870	8000
Nb-SS (current work)	2477	1400	52.3	16.2	8570	8000
Cu-SS (Liu et al., 2019; Wang et al., 2018)	1085	1400	398	16.2	8960	8000
Cu-Fe (Livne and Munitz, 1987)	1085	1538	398	80.4	8960	7870
Fe-Cu (Zhang et al., 2019)	1538	1085	80.4	398	7870	8960
SS-Fe (Mendes et al., 2013; Shi et al., 2017)	1400	1538	16.2	80.4	8000	7870
Ni-Fe[a] (Khanzadeh et al., 2012; Kosturek et al., 2019)	1455	1538	82.9	80.4	8900	7870

[a] Welds with waves difficult to define, but closer to a typical shape. Possibly in transition.

Table 8
Dissimilar welds with curled waves and their physical properties according to Gale and Totemeir (2004).

Combination (Flyer-baseplate)	Melting temperature (°C)		Thermal conductivity ($W\,m^{-1}\,K^{-1}$)		Density ($kg\,m^{-3}$)	
	Flyer	Base	Flyer	Base	Flyer	Base
Ta-Cu (Greenberg et al., 2013; Parchuri et al., 2019)	3017	1085	54.4	398	16400	8960
Al-Mg (Ghaderi et al., 2008; Yan et al., 2010)	660	650	247	155	2700	1740
Ta-SS (Paul et al., 2018b)	3017	1400	54.4	16.2	16400	8000
Ti-Fe (Chu et al., 2017; Gloc et al., 2016)	1668	1538	11.4	80.4	4510	7870
Ti-Cu (Kahraman and Gülenç, 2005)	1668	1085	11.4	398	4510	8960
Cu-W (Manikandan et al., 2011; Zhou et al., 2017)	1085	3422	398	160	8960	19300
Al-Fe (Carvalho et al., 2019a) (current work)	660	1538	247	80.4	2700	7870
Al-Nb (current work)	660	2477	247	52.3	2700	8570
Al-Cu (Carvalho et al., 2018c)	660	1085	247	398	2700	8960
Ti-SS (Manikandan et al., 2006)	1668	1400	11.4	16.2	4510	8000
Zr-Fe (Nobili and Banker, 1999; Prażmowski et al., 2017)	1855	1538	21.1	80.4	6520	7870

Table 9
Values of the impedances calculated for each welding combination, their respective IMP and wave shape.

Combination (Flyer-baseplate)	Z ($kg\,m^{-2}s^{-1} \times 10^6$)		Z_{ratio}	IMP	Type of wave	Wave forming material
	Flyer	Base				
Al-Mg (Ghaderi et al., 2008; Yan et al., 2010)	14.5	8.0	1.82	**0.82**	**Curled**	Al
Al-Cu (Carvalho et al., 2018c)	14.5	38.3	0.38	**0.62**	**Curled**	Ta
Al-Nb (current work)	14.5	36.7	0.40	**0.60**	**Curled**	Nb
Al-Fe (Carvalho et al., 2019a) (current work)	14.5	36.5	0.40	**0.60**	**Curled**	Fe
Cu-W (Manikandan et al., 2011; Zhou et al., 2017)	38.3	86.3	0.44	**0.56**	**Curled**	Ta
Ta-SS (Paul et al., 2018b)	55.6	36.4	1.53	**0.53**	**Curled**	W
Ta-Cu (Greenberg et al., 2013; Parchuri et al., 2019)	55.6	38.3	1.45	**0.45**	**Curled**	Cu
Ti-Cu (Kahraman and Gülenç, 2005)	22.0	38.3	0.58	**0.42**	**Curled**	Cu
Ti-Fe (Chu et al., 2017; Gloc et al., 2016)	22.0	36.5	0.60	**0.40**	**Curled**	Fe
Ti-SS (Manikandan et al., 2006)	22.0	36.4	0.60	**0.40**	**Curled**	SS
Zr-Fe (Nobili and Banker, 1999; Prażmowski et al., 2017)	25.4	36.5	0.69	**0.31**	**Curled**	Fe
Ni-Fe (Khanzadeh et al., 2012; Kosturek et al., 2019)	44.0	36.5	1.21	**0.21**	**Typical**[a]	Both
Cu-SS (Liu et al., 2019; Wang et al., 2018)	38.3	36.4	1.05	**0.05**	**Typical**	Both
Cu-Fe (Livne and Munitz, 1987)	38.3	36.5	1.05	**0.05**	**Typical**	Both
Fe-Cu (Zhang et al., 2019)	36.5	38.3	0.95	**0.05**	**Typical**	Both
Nb-SS (current work)	36.7	36.4	1.01	**0.01**	**Typical**	Both
Fe-SS (current work)	36.5	36.4	1.00	**0.00**	**Typical**	Both
SS-Fe (Mendes et al., 2013; Shi et al., 2017)	36.4	36.5	1.00	**0.00**	**Typical**	Both
Similar welds (Carvalho et al., 2018c, 2017)	0.0	0.0	1.00	**0.00**	**Typical**	Both

[a] Welds with waves difficult to define, but closer to a typical shape. Possibly in transition.

Kelvin–Helmholtz instability, for instance, is accepted as one of the mechanisms of wave formation in EXW. As explained by Matsuoka (2014), it is an instability at the interface of two parallel streams with relative velocity between each other. One of the reasons for the occurrence of this instability is the presence of variations in the interfacial/tangential velocity (shear flow). This discontinuity produces localised changes in pressure that lead to vorticities at the interface. The movement / flow of the material moves these vorticities. They become an unstable vortex and roll up into a spiral. The fact that differences in impedance between the materials may affect the shock wave path, behaviour and distribution at the interface, is also an indication that it could affect the interfacial phenomena that shape the waves.

Another critical piece of information resulting from these analyses is that the material forming the wave is always the material with the higher density and impedance. These morphological differences are possibly related to the way the shock waves are transmitted or reflected at the impacted interface. The physics behind these phenomena are complex, and there may also be other features that affect the wave shapes. Therefore, this aspect should be studied explicitly for further details.

These results prove that it is feasible to use both carbon steel, or niobium as interlayers for aluminium to stainless steel welds. The final

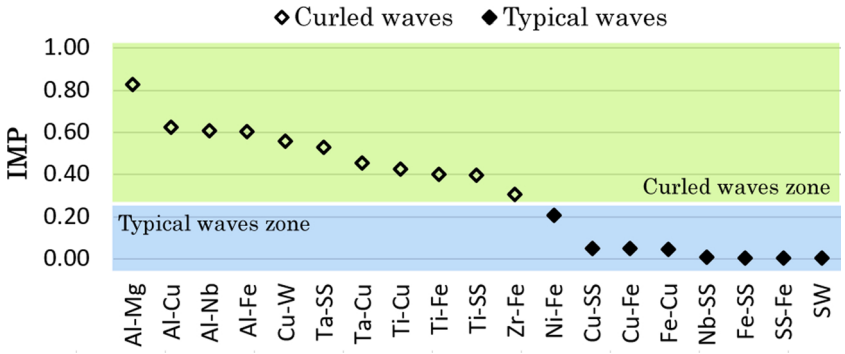

Fig. 11. Impedance mismatch parameter (IMP) for different dissimilar welds combinations and similar welds (SW).

joints using the interlayer quite improved the mechanical properties compared to both direct welding and the welding using aluminium as the interlayer from previous work. The weld using the carbon steel interlayer had the best mechanical performance. Its use should be analysed taking into account the limitations of the applicability of carbon steel (environment, corrosion resistance, among others). For particular purposes that justify its investment, niobium can be selected. In order to obtain properties more suited to a specific use or environment, different steels or niobium alloys (as long as they are similar in physical properties) can be selected.

5. Conclusions

This study has investigated the explosive welding of aluminium to stainless steel using carbon steel and niobium interlayers. Our work has led us to conclude the following points:

- The joint using carbon steel as the interlayer presented a favourable interfacial microstructure (waves on both interfaces) and better mechanical properties. All tensile-shear tests fractured outside the weld region in the weaker base material (aluminium).
- The joint using the niobium interlayer presented a favourable interfacial microstructure (waves on both interfaces). One of the tensile-shear tests fractured outside the weld region in the weaker material (aluminium) and the other test fractured near the weld region but outside the joint's interface, also in the aluminium.
- All interfaces found on both welds were wavy. However, depending on the metallic alloy combination, the shape of the wave is different.
- The results suggest that the shape of the waves is influenced by the shock impedance mismatch of the materials being welded.
- The impedance mismatch parameter (IMP) proved to be a compelling method to order metallic combinations on a single axis in order to estimate the tendency to form typical waves or curled waves.
- Typical symmetrical waves tend to form fewer IMCs than curled waves. This difference; however, was not made apparent in the mechanical tests.

Declaration of Competing Iinterests

The authors declare that they have no known competing financial interests or personal relationships that could have appeared to influence the work reported in this paper.

CRediT authorship contribution statement

G.H.S.F.L. Carvalho: Conceptualization, Methodology, Validation, Formal analysis, Investigation, Writing - original draft, Visualization. **I. Galvão:** Conceptualization, Methodology, Validation, Formal analysis, Investigation, Writing - original draft, Visualization. **R. Mendes:** Conceptualization, Methodology, Validation, Resources, Writing - review & editing, Supervision. **R.M. Leal:** Conceptualization, Methodology, Validation, Investigation, Writing - review & editing. **A. Loureiro:** Conceptualization, Methodology, Validation, Resources, Writing - review & editing, Supervision, Project administration, Funding acquisition.

Acknowledgements

This research is sponsored by FEDER funds through the program COMPETE – *Programa Operacional Factores de Competitividade* – and by national funds through FCT – *Fundação para a Ciência e a Tecnologia*, under the project UID/EMS/00285/2020.

References

Aceves, S.M., Espinosa-Loza, F., Elmer, J.W., Huber, R., 2015. Comparison of Cu, Ti and Ta interlayer explosively fabricated aluminum to stainless steel transition joints for cryogenic pressurized hydrogen storage. Int. J. Hydrogen Energy 40, 1490–1503. https://doi.org/10.1016/j.ijhydene.2014.11.038.

ASM Handbook, 1990a. Volume 2 - Properties and selection: nonferrous alloys and special-purpose materials. ASM Metals Handbook, 10th ed. ASM International, Materials Park, Ohio, USA.

ASM Handbook, 1990b. Volume 1 - Properties and selection: irons, steels, and high performance alloys. ASM Metals Handbook, 10th ed. ASM International, Materials Park, Ohio, USA.

Banker, J.G., Reineke, E.G., 1993. Explosion welding. ASM Handbook — Volume 6: Welding, Brazing and Soldering. ASM International, Materials Park, Ohio, USA, pp. 303–305. https://doi.org/10.31399/asm.hb.v06.a0001376.

Carvalho, G.H.S.F.L., Mendes, R., Leal, R.M., Galvão, I., Loureiro, A., 2017. Effect of the flyer material on the interface phenomena in aluminium and copper explosive welds. Mater. Des. 122, 172–183. https://doi.org/10.1016/j.matdes.2017.02.087.

Carvalho, G.H.S.F.L., Galvão, I., Mendes, R., Leal, R.M., Loureiro, A., 2018a. Explosive welding of aluminium to stainless steel. J. Mater. Process. Technol. 262, 340–349. https://doi.org/10.1016/j.jmatprotec.2018.06.042.

Carvalho, G.H.S.F.L., Galvão, I., Mendes, R., Leal, R.M., Loureiro, A., 2018b. Formation of intermetallic structures at the interface of steel-to-aluminium explosive welds. Mater. Charact. 142, 432–442. https://doi.org/10.1016/j.matchar.2018.06.005.

Carvalho, G.H.S.F.L., Galvão, I., Mendes, R., Leal, R.M., Loureiro, A., 2018c. Influence of base material properties on copper and aluminium–copper explosive welds. Sci. Technol. Weld. Join. 23, 501–507. https://doi.org/10.1080/13621718.2017.1417783.

Carvalho, G.H.S.F.L., Galvão, I., Mendes, R., Leal, R.M., Loureiro, A., 2019a. Microstructure and mechanical behaviour of aluminium-carbon steel and aluminium-stainless steel clads produced with an aluminium interlayer. Mater. Charact. 155, 109819. https://doi.org/10.1016/j.matchar.2019.109819.

Carvalho, G.H.S.F.L., Galvão, I., Mendes, R., Leal, R.M., Loureiro, A., 2019b. Weldability of aluminium-copper in explosive welding. Int. J. Adv. Manuf. Technol. 103, 3211–3221. https://doi.org/10.1007/s00170-019-03841-9.

Chadwick, M.D., Jackson, P.W., 1983. Explosive welding in planar geometries. In: Blazynski, T.Z. (Ed.), Explosive Welding, Forming and Compaction. Springer, Netherlands, Dordrecht, pp. 219–287. https://doi.org/10.1007/978-94-011-9751-9_7.

Chen, X., Chandra, N., 2004. The effect of heterogeneity on plane wave propagation through layered composites. Compos. Sci. Technol. 64, 1477–1493. https://doi.org/10.1016/j.compscitech.2003.10.024.

Chu, Q., Zhang, M., Li, J., Yan, C., 2017. Experimental and numerical investigation of microstructure and mechanical behavior of titanium/steel interfaces prepared by explosive welding. Mater. Sci. Eng. A 689, 323–331. https://doi.org/10.1016/j.msea.2017.02.075.

Crossland, B., 1982. Explosive Welding of Metals and Its Application, 1st ed. Oxford University Press, New York, USA.

El-Sobky, H., 1983. Mechanics of explosive welding. In: Blazynski, T.Z. (Ed.), Explosive Welding, Forming and Compaction. Springer, Netherlands, Dordrecht, pp. 189–217. https://doi.org/10.1007/978-94-011-9751-9_6.
Gale, W.F., Totemeir, T.C., 2004. General physical properties. In: Gale, W.F., Totemeir, T.C. (Eds.), Smithells Metals Reference Book. Elsevier, Oxford, England. https://doi.org/10.1016/B978-075067509-3/50017-8. pp. 14-1–14-45.
Ghaderi, S.H., Mori, A., Hokamoto, K., 2008. Analysis of explosively welded aluminum–AZ31 magnesium alloy joints. Mater. Trans. 49, 1142–1147. https://doi.org/10.2320/matertrans.MC200796.
Gloc, M., Wachowski, M., Plocinski, T., Kurzydlowski, K.J., 2016. Microstructural and microanalysis investigations of bond titanium grade1/low alloy steel st52-3N obtained by explosive welding. J. Alloys. Compd. 671, 446–451. https://doi.org/10.1016/j.jallcom.2016.02.120.
Grady, D., 2017. Shocks and structured waves. Physics of Shock and Impact, vol. 1 IOP Publishing Ltd.https://doi.org/10.1088/978-0-7503-1254-7ch1. pp. 1.1–1.103.
Greenberg, B.A., Ivanov, M.A., Rybin, V.V., Elkina, O.A., Antonova, O.V., Patselov, A.M., Inozemtsev, A.V., Plotnikov, A.V., Volkova, A.Y., Besshaposhnikov, Y.P., 2013. The problem of intermixing of metals possessing no mutual solubility upon explosion welding (Cu–Ta, Fe–Ag, Al–Ta). Mater. Charact. 75, 51–62. https://doi.org/10.1016/j.matchar.2012.10.011.
Guo, X., Tao, J., Wang, W., Li, H., Wang, C., 2013. Effects of the inner mould material on the aluminium-316L stainless steel explosive clad pipe. Mater. Des. 49, 116–122. https://doi.org/10.1016/j.matdes.2013.02.001.
Guo, X., Fan, M., Wang, L., Ma, F., 2016a. Bonding interface and bending deformation of Al/316LSS clad metal prepared by explosive welding. J. Mater. Eng. Perform. 25, 2157–2163. https://doi.org/10.1007/s11665-016-2057-9.
Guo, X., Wang, H., Liu, Z., Wang, L., Ma, F., Tao, J., 2016b. Interface and performance of CLAM steel/aluminum clad tube prepared by explosive bonding method. Int. J. Adv. Manuf. Technol. 82, 543–548. https://doi.org/10.1007/s00170-015-7380-z.
Hokamoto, K., Izuma, T., Fujita, M., 1993. New explosive welding technique to weld aluminum alloy and stainless steel plates using a stainless steel intermediate plate. Metall. Trans. A 24, 2289–2297. https://doi.org/10.1007/BF02648602.
Hoseini Athar, M.M., Tolaminejad, B., 2015. Weldability window and the effect of interface morphology on the properties of Al/Cu/Al laminated composites fabricated by explosive welding. Mater. Des. 86, 516–525. https://doi.org/10.1016/j.matdes.2015.07.114.
Kahraman, N., Gülenç, B., 2005. Microstructural and mechanical properties of Cu–Ti plates bonded through explosive welding process. J. Mater. Process. Technol. 169, 67–71. https://doi.org/10.1016/j.jmatprotec.2005.02.264.
Kakimoto, E., 2000. Joint material of aluminium and stainless steel for welding. Weld. Int. 14, 614–619. https://doi.org/10.1080/09507110009549238.
Kennedy, J.E., 1970. Gurney Energy of Explosives: Estimation of the Velocity and Impulse Imparted to Driven Metal, Report No. SC-RR-70-790. Sandia Laboratories, New Mexico, USA.
Khanzadeh, M.R., Akbari Mousavi, S.A.A., Amadeh, A., Liaghat, G.H., 2012. Correlation between numerical finite element simulation and experiments for explosive cladding of nickel base super alloy on hot tool steel. Strain 48, 342–355. https://doi.org/10.1111/j.1475-1305.2011.00828.x.
Kosturek, R., Wachowski, M., Śnieżek, L., Gloc, M., 2019. The influence of the post-weld heat treatment on the microstructure of inconel 625/carbon steel bimetal joint obtained by explosive welding. Metals (Basel) 9, 246. https://doi.org/10.3390/met9020246.
Leitão, C., Galvão, I., Leal, R.M., Rodrigues, D.M., 2012. Determination of local constitutive properties of aluminium friction stir welds using digital image correlation. Mater. Des. 33, 69–74. https://doi.org/10.1016/j.matdes.2011.07.009.
Liu, Y., Li, C., Hu, X., Yin, C., Liu, T., 2019. Explosive welding of copper to high nitrogen austenitic stainless steel. Metals (Basel) 9, 339. https://doi.org/10.3390/met9030339.
Livne, Z., Munitz, A., 1987. Characterization of explosively bonded iron and copper plates. J. Mater. Sci. 22, 1495–1500. https://doi.org/10.1007/BF01233153.
Manikandan, P., Hokamoto, K., Deribas, A.A., Raghukandan, K., Tomoshige, R., 2006. Explosive welding of titanium/stainless steel by controlling energetic conditions. Mater. Trans. 47, 2049–2055. https://doi.org/10.2320/matertrans.47.2049.
Manikandan, P., Lee, J.O., Mizumachi, K., Mori, A., Raghukandan, K., Hokamoto, K., 2011. Underwater explosive welding of thin tungsten foils and copper. J. Nucl. Mater. 418, 281–285. https://doi.org/10.1016/j.jnucmat.2011.07.013.
Matsuoka, C., 2014. Kelvin-Helmholtz instability and roll-up. Scholarpedia 9, 11821. https://doi.org/10.4249/scholarpedia.11821.
Matthews, S.J., Howden, D.G., Bratkovich, N.F., King, J.F., 1982. Dissimilar metals. AWS Welding Handbook: Volume 4 — Metals and Their Weldability. American Welding Society, USA, pp. 513–547.
Mendes, R., Ribeiro, J.B., Loureiro, A., 2013. Effect of explosive characteristics on the explosive welding of stainless steel to carbon steel in cylindrical configuration. Mater. Des. 51, 182–192. https://doi.org/10.1016/j.matdes.2013.03.069.
Mendes, R., Ribeiro, J., Plaksin, I., Campos, J., Tavares, B., 2014. Differences between the detonation behavior of emulsion explosives sensitized with glass or with polymeric micro-balloons. J. Phys. Conf. Ser. 500, 1–6. https://doi.org/10.1088/1742-6596/500/5/052030.
Nobili, A., Banker, J., 1999. Recent developments in zirconium-steel explosion clad. Proc. 1999 React. Met. Corros. Appl. Conf. 83–88.
Ouyang, J., Yarrapareddy, E., Kovacevic, R., 2006. Microstructural evolution in the friction stir welded 6061 aluminum alloy (T6-temper condition) to copper. J. Mater. Process. Technol. 172, 110–122. https://doi.org/10.1016/j.jmatprotec.2005.09.013.
Parchuri, P., Kotegawa, S., Yamamoto, H., Ito, K., Mori, A., Hokamoto, K., 2019. Benefits of intermediate-layer formation at the interface of Nb/Cu and Ta/Cu explosive clads. Mater. Des. 166, 107610. https://doi.org/10.1016/j.matdes.2019.107610.
Patterson, R.A., 1993. Fundamentals of explosion welding. ASM Handbook — Volume 6: Welding, Brazing and Soldering. ASM International, Materials Park, Ohio, USA, pp. 160–164. https://doi.org/10.31399/asm.hb.v06.a0001351.
Paul, H., Lityńska-Dobrzyńska, L., Prazmowski, M., 2013. Microstructure and phase constitution near the interface of explosively welded aluminum/copper plates. Metall. Mater. Trans. A 44, 3836–3851. https://doi.org/10.1007/s11661-013-1703-1.
Paul, H., Maj, Ł., Prażmowski, M., Gałka, A., Miszczyk, M., Petrzak, P., 2018a. Microstructure and mechanical properties of multi-layered Al/Ti composites produced by explosive welding. Procedia Manuf. 15, 1391–1398. https://doi.org/10.1016/j.promfg.2018.07.343.
Paul, H., Miszczyk, M.M., Chulist, R., Prażmowski, M., Morgiel, J., Gałka, A., Faryna, M., Brisset, F., 2018b. Microstructure and phase constitution in the bonding zone of explosively welded tantalum and stainless steel sheets. Mater. Des. 153, 177–189. https://doi.org/10.1016/j.matdes.2018.05.014.
Prażmowski, M., Rozumek, D., Paul, H., 2017. Static and fatigue tests of bimetal Zr-steel made by explosive welding. Eng. Fail. Anal. 75, 71–81. https://doi.org/10.1016/j.engfailanal.2016.12.022.
Shi, C., Yang, X., Ge, Y., You, J., Hou, H., 2017. Lower limit law of welding windows for explosive welding of dissimilar metals. J. Iron Steel Res. Int. 24, 852–857. https://doi.org/10.1016/S1006-706X(17)30126-7.
Spittel, M., Spittel, T., 2009. Steel symbol/number: DC06/1.0873. In: Warlimont, H. (Ed.), Landolt-Börnstein - Group VIII - Metal Forming Data of Ferrous Alloys - Deformation Behaviour. Springer, Berlin Heidelberg, Berlin, Heidelberg, pp. 312–317. https://doi.org/10.1007/978-3-540-44760-3_43.
Wang, Y., Li, X., Wang, X., Yan, H., 2018. Fabrication of a thick copper-stainless steel clad plate for nuclear fusion equipment by explosive welding. Fusion Eng. Des. 137, 91–96. https://doi.org/10.1016/j.fusengdes.2018.08.017.
Yan, Y.B., Zhang, Z.W., Shen, W., Wang, J.H., Zhang, L.K., Chin, B.A., 2010. Microstructure and properties of magnesium AZ31B-aluminum 7075 explosively welded composite plate. Mater. Sci. Eng. A 527, 2241–2245. https://doi.org/10.1016/j.msea.2009.12.007.
Zhang, H., Jiao, K.X., Zhang, J.L., Liu, J., 2019. Comparisons of the microstructures and micro-mechanical properties of copper/steel explosive-bonded wave interfaces. Mater. Sci. Eng. A 756, 430–441. https://doi.org/10.1016/j.msea.2019.04.064.
Zhou, Q., Feng, J., Chen, P., 2017. Numerical and experimental studies on the explosive welding of tungsten foil to copper. Materials (Basel) 10, 984. https://doi.org/10.3390/ma10090984.